Sains Malaysiana 44(11)(2015): 1551–1559

Preparation of Durian Skin Nanofibre (DSNF) and Its Effect on the Properties of Polylactic Acid (PLA) Biocomposites

(Penyediaan Nano-serabut Kulit Durian (DSNF) dan Kesannya ke atas Sifat Biokomposit Asid Polilaktik (PLA))

M.N. Nur Aimi*, H. Anuar, M. Maizirwan, S.M. Sapuan, M.U. Wahit & S. Zakaria

ABSTRACT

Biological fermentation of Rhizopus oryzae *was introduced to extract cellulose nanofibre from durian skin fibre (DSF). The diameter of the extracted durian skin nanofibre (DSNF) was in the range of 49-81 nm. The changes of chemical composition of DSNF were clearly seen after evaluated via TAPPI standard test methods. Verification via Fourier transform infrared (FTIR) confirmed the deduction of hemicelluloses and lignin in DSNF in the range of 1200 to 1000 cm^{-1}. X-ray diffraction (XRD) demonstrated increment in the crystallinity from 58.3 to 72.2% after biological fermentation. DSNF was then incorporated into polylactic acid (PLA) via extrusion and injection moulding processes. The effect of 1-5 wt. % DSNF content on PLA biocomposites was investigated for its mechanical and thermal properties. The presence of only 1 wt. % improved the tensile and impact strength by 14.1 MPa and 33.1 kJ/m^2, respectively. The thermal properties of PLA-1DSNF biocomposite also recorded higher thermal stability, glass transition temperature (T_g), crystallization temperature (T_c) and melting temperature (T_m). Additionally, from the DMA, it was determined that PLA-1DSNF possessed lower storage modulus and loss modulus, as well as low energy dissipation.*

Keywords: Biocomposites; durian skin fibre; durian skin nanofiber; polylactic acid

ABSTRAK

Fermentasi biologi Rhizopus oryzae *telah diperkenalkan bagi mengekstrak nano-serabut selulosa daripada serabut kulit durian (DSF). Diameter nano-serabut kulit durian (DSNF) adalah dalam julat 49-81 nm. Ujian piawaian kaedah TAPPI menunjukkan perubahan komposisi kimia DSNF. Pengesahan melalui transformasi Fourier inframerah (FTIR) menunjukkan pengurangan hemiselulosa dan lignin sekitar 1200 hingga 1000 cm^{-1}. Pembelauan sinar-X (XRD) menunjukkan peningkatan hablur daripada 58.3 kepada 72.2% selepas fermentasi biologi. Seterusnya, DSNF telah ditambahkan kepada asid polilaktik (PLA) melalui pemprosesan secara penyemperitan dan pengacuanan suntikan. Kesan kemasukan DSNF daripada 1-5 wt. % ke atas sifat mekanik dan terma biokomposit PLA telah dikaji. Kehadiran DSNF serendah 1 wt. % memperbaiki kekuatan regangan dan hentaman, masing-masing sebanyak 14.1 MPa dan 33.1 kJ/m^2. Sifat terma bio komposit PLA-1DSNF juga merekodkan kestabilan terma, suhu peralihan kaca (T_g), suhu penghabluran (T_c) dan suhu peleburan (T_m) yang lebih tinggi. Analisis daripada DMA menunjukkan PLA-1DSNF mempunyai modulus simpanan dan kehilangan yang lebih rendah, juga kehilangan tenaga yang rendah.*

Kata kunci: Asid polilaktik; biokomposit; nano-serabut kulit durian; serabut kulit durian

Introduction

The accessibility, plenty and positive characteristics of natural fibres have led to progressive research into their utilization in the composites industries. Natural fibres are known for being low cost, light, renewable, less abrasive to the environment and risk-free (Mamun & Bledski 2013). Bamboo, kenaf, jute, flax, hemp and cotton are among the common natural fibres reported as reinforcing materials. Recently, durian skin fibre (DSF) has been reported to be a promising agricultural biofiller in the composites industries (Manshor et al. 2014). They concluded that the physical behaviour, crystallinity and chemical structures of DSF are within the properties of other fruit fibres. Durian scientifically known as *Durio zibethinus Murray,* consists of DSF and seed. Both are the waste generated about 60-70% of durian fruit. It is well known that durian will produce a notorious smell; however, after the separation process into DSF, the odour begins to fade as the process is conducted at high temperature in an oven during the drying process (Nur Aimi et al. 2014).

The utilization of nano- and micro-sized natural fibre reinforced biodegradable polymers is of significant benefit as it reduces dependency on foreign petroleum resources and is an alternative to alleviating the disposal problems of composites. Besides, the presence of nano-sized agricultural biomass as filler in the polymer offers remarkable advantages to green composites or biocomposites. These include increased surface-area-to-volume ratio, lower density and high flexibility in comparison to the micro-size of the same fibre (Albert et al. 2011) Cellulose nanofibre can be prepared in several ways, including chemical, mechanical and biological

treatments. Among these methods, biological fermentation is attractive because it involves natural degradation of the fibres using endogenous enzymes or micro-organisms. Apart from promoting green technology, this method is also environmentally friendly, as it consumes only low energy and chemicals (Atta & Yassen 2014). Besides acquiring the nanofibre, value added biochemical products such as ethanol and lactic acid may also be produced during biological fermentation.

Hence, this study focused on the extraction and preparation of durian skin nanofibre (DSNF) from DSF through biological treatment via fermentation of *Rhizopus oryzae*. The obtained DSNF was then incorporated into polylactic acid (PLA) using conventional plastic processing machines. The effect of DSNF loadings on PLA biocomposites were investigated for their mechanical, thermal and morphological properties.

Materials and Methods

Collection of Samples

In this study, PLA was bought from NatureWorks®, China (grade 3051D). The density, melting temperature and glass transition temperature of PLA are 0.998 g/cm^3, 152.3ºC and 57-61ºC, respectively. Durian skin waste was collected from Pahang, Malaysia. It was washed, chopped, ground and dried in an oven at 105ºC for 24 h.

Preparation of the DSNF

DSNF was produced from the mechanical pre-treatment of DSF that was previously chopped, ground and sieved into 100-250 μm mesh-size. Then, it was further biologically treated by means of the fermentation process of *Rhizopus oryzae*. *Rhizopus oryzae* used in this experiment is a type of fungi that is naturally occurred from the expired bread and its strain with reference collection of American type culture collection (ATCC). It was sporulated and grown on potato dextrose agar (PDA) and stored at 37ºC for 3 days. Potato dextrose broth (PDB) was chosen as the medium for fermentation, prepared with controlled pH6 and sterilized in an autoclaved at 121ºC. The biological treatment started as *Rhizopus oryzae* grown on PDA was first collected by shaving using L-loop and extracting it with 25 mL sterilized distilled water. The inoculum size was 2-5 × 10^5 spores mL^{-1}. Then, the inoculums were added into 250 mL Erlenmeyer flasks containing 1 g DSF, 50 mL PDB and 50 mL deionized water. The biological fermentation process was conducted at 25ºC for 7 days with an agitation speed of 250 rpm (Nur Aimi et al. 2011).

Chemical Properties Analysis of DSF and DSNF

The compositions of hollocellulose and α-cellulose for DSF and DSNF were analyzed using TAPPI test methods T249-75 and T203 om-99, respectively. The composition of insoluble and soluble lignin was assessed using TAPPI T222 om-88 and TAPPI UM-250 accordingly. Total of lignin was calculated by the addition of soluble and insoluble lignin. The content of hemicellulose was calculated using (1). An average of three samples were tested and calculated for each analysis.

$$Hemicelluso = Holocellulose - Cellulose. \quad (1)$$

The extractive and ash content were analysed via TAPPI T204 om-88 and T211 om-93, respectively.

Physical Properties Analysis of DSF and DSNF

A Fei Quanta 200 scanning electron microscope (SEM) was used to measure the DSF and DSNF dimension. Knowing the length and diameter of the fibre, the aspect ratio of the DSF and DSNF was calculated. About 50 fibres were taken for measurement. To verify its size, the analysis of particle size distribution of DSNF was then conducted using dynamic light scattering via zeta sizer (zeta-sizer nano-S, Malvern, England) according to the ISO 13320:2009 standard. The structure and sizes of the DSNF were further analysed using a transmission electron microscope (TEM, CM12 Phillips, USA) with field emission. Fourier transform infrared (FTIR) analysis was conducted to track the changes of the functional groups of DSF and DSNF using a Spectrum 100 Perkin Elmer spectrometer with spectra recorded wavenumbers from 4000 to 380 cm^{-1} in the transmission mode. The structure, phase and crystallinity of the DSF and DSNF were determined using a Shimadzu X-ray diffractometer (XRD 6000) machine. The diffracted intensity of CuK_α (wavelength of 0.1542 nm) was recorded between 10º and 35º (2θ angle range) at 50 kV and 40 mA. The crystallinity index (CI) of the DSF and DSNF was calculated (Segal et al. 1959).

Preparation of PLA-DSNF Biocomposites

PLA and DSNF were extruded using a Thermo Haake twin screw extruder. The temperature during the extrusion process was 180ºC and the screw speed was 100 rpm. The compositions and designation of the prepared PLA-DSNF biocomposites are shown in Table 1.

TABLE 1. Compositions and designation of PLA-DSNF biocomposites

Designation	Matrix (wt. %)	Nanofiller (wt. %)
PLA	100	0
PLA-1DSNF	99	1
PLA-2DSNF	98	2
PLA-3DSNF	97	3
PLA-4DSNF	96	4
PLA-5DSNF	95	5

Tensile tests were conducted in accordance with ASTM D638-10 using a universal testing machine (LLOYD). The load cell was 10 kN and the crosshead speed was 50 mm/min. The Charpy impact test was performed as per ASTM

D256-10 on a Dynisco Polymer Test, Simatic OP7 machine. The velocity and weight of the hammer were 3.67 m/s and 0.898 kg. Thermogravimetry analysis (TGA) was carried out using a TA Instruments TGA Q500 analyser based on ASTM D3850. About 8-10 mg of biocomposites was used for the TGA analysis. The analysis was carried out from 25 to 500°C with a heating rate of 10°C min^{-1}. The differential scanning calorimetry (DSC) was studied using a TA Instruments DSC Q1000 analyser according to ASTM E1356. The temperature setting for DSC ranges from 25 to 300°C. The enthalpy of crystallization (ΔH_c), the enthalpy of fusion (ΔH_m) and the crystallinity (X_c %) were calculated using (2).

$$X_c\% = \frac{\Delta H_m - \Delta H_c}{93.1} \times 100, \quad (2)$$

where ΔH_m is the enthalpy of fusion and ΔH_c is the enthalpy of crystallization. ΔH_o, the enthalpy of fusion of a perfect 100% crystalline is taken as 93 J/g. The distribution of nanofibres in the composites was also examined using TEM. The storage modulus and loss modulus, as well as the glass transition temperature (T_g) was then characterized by the dynamic mechanical analysis (Pyris Diamond DMA, Perkin Elmer, USA) via ASTM D7028 standard.

Results and Discussion

Chemical composition, morphological, size and dimension analysis

The cellulose, hemicellulose and lignin constituents in DSF and DSNF are presented in Table 2. It can be seen from Table 2 that the cellulose content in DSNF is about 2% lower than in DSF. The hemicellulose and lignin content in DSNF, however, decreased by 50 and 30%, respectively, relative to DSF. The extractive for DSNF increased from 1.5 to 7.2% as it is the phytochemicals components of the fibre such as alkaloids, flavonoids and tannins that aroused when the cellulose structure was degraded and hemicelluloses as well as lignin were effectively removed. The analysis confirmed the effectiveness of *Rhizopus oryzae* to degrade the cellulose structure in the DSF by producing several enzymes used to eliminate the hydrogen bond in the cellulose and hydrolysed the hemicellulose and lignin components in the fibres (Janardhnan & Sain 2011). Besides, low hemicelluloses content of the fibre may not absorb more moisture and will not degrade at a lower temperature (Sahan 2011). Thus, the removal hemicelluloses and lignin for this case illustrates its advantages for structural applications.

The micrographs in Figure 1(a)-1(b) shows the DSF and Figure 1(c)-1(d) shows the DSNF. The micrographs in Figure 1(a) and 1(c) are at 1000× magnification whereas Figure 1(b) and 1(d) are at 1500× magnification. The observed surface of DSF is complex in structure as the fibrils are associated with the bundle form rather than the surface of the fermented fibres. The complex structure of DSF is due to the existence of cellulose, hemicellulose and lignin. It can be seen in Figure 1(c)-1(d) that biological treatment separated the fibres into individual fibres and showed the reduction in the diameter of DSNF.

Any microorganism which includes *Rhizopus oryzae* that was naturally generated from the expired bread was well established in terms of its bioassay activity. This will produce biochemical products indirectly to extract cellulose into nanosize that involved many sugar metabolism pathways such as glycolysis and pyruvate metabolism. Biologically, *Rhizopus oryzae* was grown, consumed, degraded and modified the DSF structure into nanosize with the aid of endogenous enzymes and completed the consumption of nutrients in 7 days fermentation. These 7 days of fermentation was chosen on the basis of lactic acid production (Nur Aimi et al. 2011). This is also in agreement with the studies of nanocellulose via microorganism isolated from citrus processing orange waste (Tsukamoto et al. 2013).

Comparison of the diameters, lengths and aspect ratios for both DSF and DSNF are presented in Table 3. As reported earlier, diameter and length of DSF are longer than DSNF, thus contributing to lower aspect ratio of DSF (Manshor et al. 2014). However, upon fermentation, the diameter and length for DSNF reduced to 49-81 nm and 1.2-3.1 μm, respectively. The average aspect ratio for DSNF thus increased to 33. The diameter of the DSF reduced significantly after fermentation or biological treatment as the *Rhizopus oryzae* attacked the surface of the fibre simultaneously consuming it as a carbon source. This is consistent with the results where the nanofibres isolated from kenaf core fibres were reported with diameters in the range of 20-25 nm and several thousand nanometers in length (Isroi et al. 2011). Additionally, it was reported that nanowhiskers from wood have lengths, diameters and aspect ratios in the range 105-150, 4.9-12 and 10-30, respectively (Jonoobi et al. 2011).

The TEM image of DSNF is presented in Figure 2. The assessment of isolated nanofibres confirms the existence of nanofibre and its aggregates. Due to the aggregation of samples during the fermentation process, there was a mix of DSF and DSNF with diameters larger than 100 nm. Geometrical features such as size, dimensions and the shapes of the nanofibres produced depend on the nature of

TABLE 2. Chemical composition of DSF and DSNF

	Cellulose (%)	Hemicellulose (%)	Lignin (%)	Extractive (%)	Ash (%)
DSF	68.1±0.5	16.2±0.5	13.7±0.5	1.5±0.5	0.5±0.5
DSNF	66.5±0.5	15.7±0.5	10.6±0.5	7.2±0.5	-

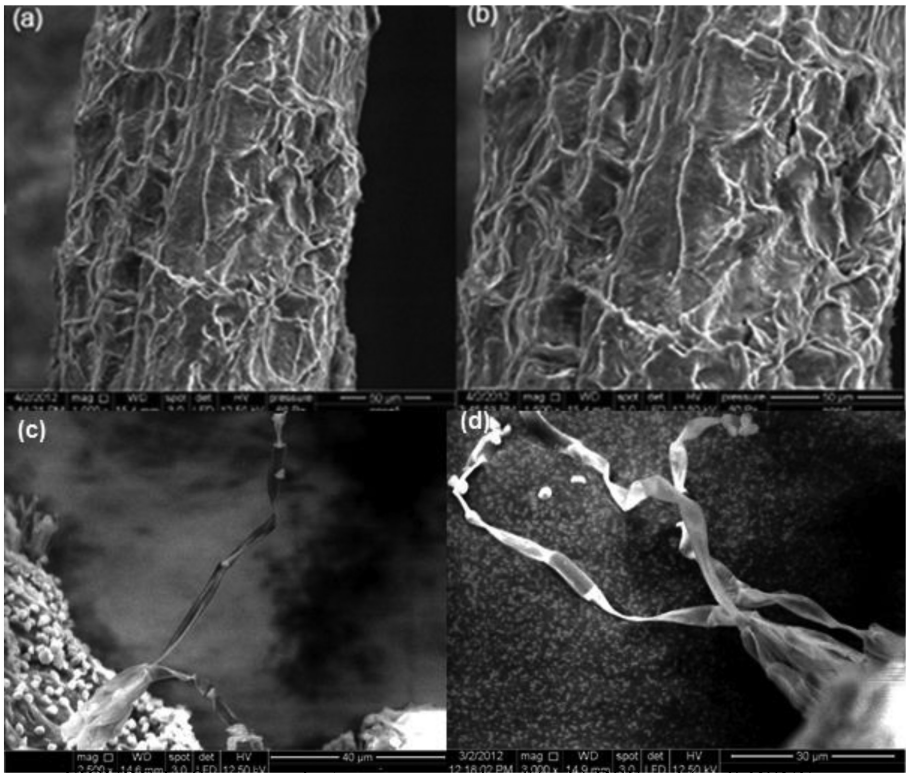

FIGURE 1. Scanning electron micrographs of (a–b) DSF and (c–d) DSNF

TABLE 3. Diameter, length and aspect ratio of DSF and DSNF

	DSF (Manshor et al. 2014)			DSNF		
	Diameter, D (μm)	Length, L (mm)	Aspect ratio (L/D)	Diameter, D (nm)	Length, L (μm)	Aspect ratio (L/D)
Min	170	0.84	4.94	49	1.2	25
Max	447	2.38	5.32	81	3.1	38
Average	309	1.61	5.21	63	2.08	33

the cellulose sources as well as the fermentation conditions such as time, temperature and purity of the materials (Eicchorn et al. 2010). As observed in Figure 2, the cross sections of the fibres were inconsistent and the fibres were still in the form of a bundle. This can be associated with the attachment of the spores from the *Rhizopus oryzae* on the surface of the fibres and the agglomeration of fibre still occurred. The improvement of DSNF and DSF are clearly seen due to the removal of hemicelluloses and lignin through mechanical study that had been discussed further next.

The FTIR spectra for cellulose, hemicelluloses and lignin were widely reported in open literature where it consists mainly of esters, ketones, alkanes, aromatics and alcohols with varied ranges of functional groups (Siqueira et al. 2010). These three main components are showed through FTIR in Figure 3. The obvious absorption band of O-H stretching and C-H vibration can be seen around 3400 to 2800 cm^{-1} for DSF and DSNF spectra. These peaks indicate the main characteristics of cellulose which are 3409 and

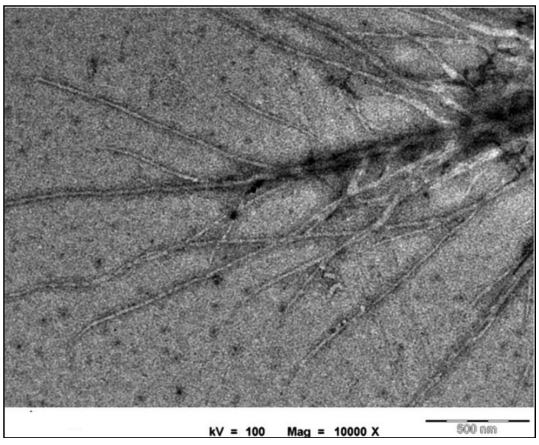

FIGURE 2. Transmission electron micrographs of DSNF

3384 cm^{-1} as well as 2844 and 2836 cm^{-1} for DSF and DSNF, respectively. The absorption bands around 1634 and 1651 cm^{-1} in DSF and DSNF, respectively, are associated with C-O

stretching which contains acetyl group and ester linkage of carbonyl group of hemicelluloses and lignin. The presence of 1400 to 1300 cm^{-1} region suggested the CH deformation vibrations of CH_2 from cellulose. The absorption band at 1200 to 1000 cm^{-1} region may possibly be due to C=O and aromatic stretching from lignin (Ibrahim et al. 2010). Table 4 shows the summary of possible infrared transmittance that was observed in DSF and DSNF.

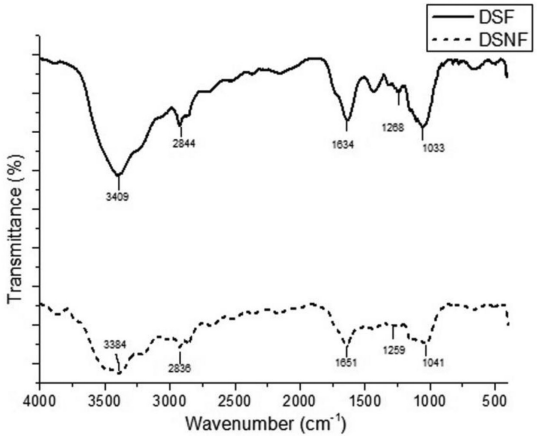

FIGURE 3. FTIR spectra of DSF and DSNF

The X-ray diffractograph for DSF and DSNF is shown in Figure 4. The CI values calculated for DSF and DSNF were 58.3 and 72.2%, respectively. A higher CI value was recorded for DSNF as its major crystalline peak at 2θ is 22° due to the reduction amount of amorphous components during biological treatment. In other studies by Chen et al. (2011) and Dasong and Mizi (2010) also reported that the degree of crystallinity for fibres was increased after the isolation of nanofibres due to the delignification process which is believed to occurred as the crystalline cellulose was arranged orderly. Theoretically, higher crystallinity of the fibre enhances the mechanical properties of the composites (Kazimierczak et al. 2012).

TENSILE AND IMPACT PROPERTIES OF PLA-DSNF BIOCOMPOSITES

The effect of DSNF content on the tensile properties of PLA biocomposites is shown in Figure 5. The unfilled PLA recorded a lower tensile strength and modulus at 42 and 1398 MPa, respectively. The incorporation of 1 wt. % DSNF amplified the tensile strength of PLA biocomposite

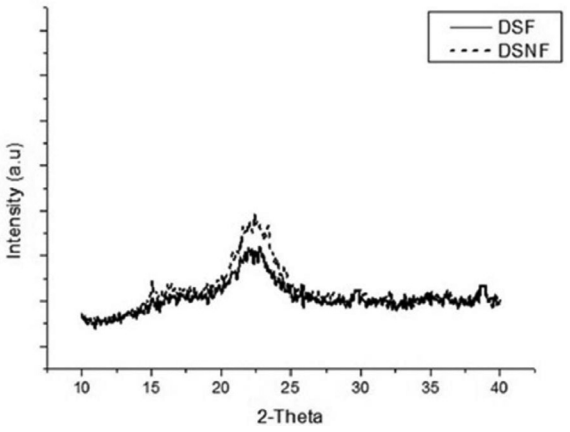

FIGURE 4. X-ray diffractograph for DSF and DSNF

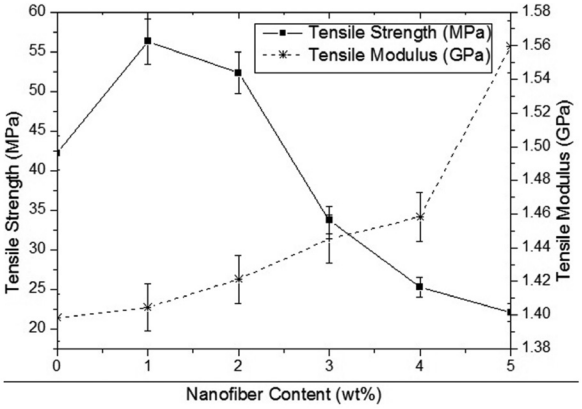

FIGURE 5. The effect of DSNF content on the tensile properties of PLA biocomposite

by about 33% as compared to the PLA matrix. The tensile strength of the biocomposites, however, decreased as 2 to 5 wt. % of DSNF was added to the PLA. Figure 5 also illustrates the tensile modulus of PLA and its biocomposites. In general, the tensile modulus of the biocomposites increased significantly with the increased in DSNF content from 0 to 5 wt. %.

Figure 6 exhibits the effect of DSNF content on the impact strength of PLA and its biocomposites. A similar trend to tensile strength was noted for the impact strength of PLA biocomposite. The presence of 1 wt. % DSNF enlarged the impact strength of the PLA biocomposite compared to unfilled PLA. The impact strength however decreased beyond 2 wt. % DSNF. The impact strength for PLA-DSNF biocomposites is, however, significantly higher than that

TABLE 4. Summary of infrared transmittance peak of DSF and DSNF

	O-H stretching	C-H vibration	C=O stretching	C-O Stretching	C-C stretching
DSF	3409	2844	1651	1268	1033
DSNF	3384	2836	1634	1259	1041

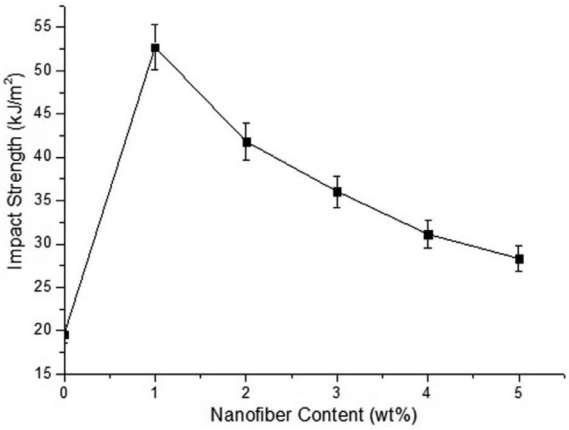

FIGURE 6. The effect of DSNF content on the impact strength of PLA biocomposite

of PLA reinforced with 30 wt. % DSF (Manshor et al. 2014). The improvement in the tensile and impact properties shows the ability of DSNF to impart greater strength and stiffness to the PLA biocomposites. The higher CI value due to the reduction amount of amorphous components could be associated with the inherent stiffness of the DSNF that positively contributes to the overall properties of the composites. It can be inferred that the biological method used to extract nanofibre from DSF created a hairy fibre or nanofibrillated cellulose. This nanosize fibre is expected to promote interlocking adhesion between DSNF and the PLA matrix as can be observed in the SEM micrographs in Figure 7. The micrograph in Figure 7 also shows the existence of cracks which indicates transition from ductile to brittle behaviour as the biocomposite underwent tensile testing. The removal of the amorphous components consisting of lignin and hemicelluloses during fermentation resulted in a lower density and a rigid interfibrillar region.

The optimum strength obtained in PLA-1DSNF was capable of arranging the nanofibres along the direction of the tensile and impact deformation due its higher aspect ratio, as seen in Table 2, thus provides a larger surface area. Decrements in tensile and impact strength occurred in the DSNF content beyond 2 wt. % could be associated with the reduced mobility of the polymer matrix in absorbing more energy with the higher fibre content (Mohammad & Arsad 2013; Siyamak et al. 2012).

THERMAL PROPERTIES OF PLA-DSNF COMPOSITES

The effect of temperature on the weight loss of the PLA matrix was compared with the optimum value obtained from the mechanical test which is PLA-1DSNF biocomposite. It was analysed by TGA. PLA and biocomposite possess two degradation zones, as illustrated in the TGA curve in Figure 8. The first degradation zone can be correlated to cellulose, hemicellulose and lignin, while the second is associated with the depolymerization of PLA (Meng et al. 2011).

The initial decomposition temperature at 15% weight loss ($T_{15\%}$), final decomposition temperature (T_f) and percentage of char residue at 600°C are presented in Table 5. Based on Table 5, comparing the T_i for PLA-1DSNF to PLA, the biocomposite is 4°C higher than the PLA matrix. This shows that the thermal stability of PLA is enhanced with DSNF. With increasing temperature, the T_f for biocomposite is 4°C lower than that of PLA which is evidence of the weak thermal stability of biocomposite. This could be due to the fact that thermal decomposition for cellulosic materials, composed of cellulose, hemicellulose and lignin, occurred at temperatures around 200 to 400°C (Kaiser et al. 2013; Kumar & Awasthi 2014). Char residue for PLA-1DSNF is also higher compared to the PLA matrix owing to the non-existence of volatile

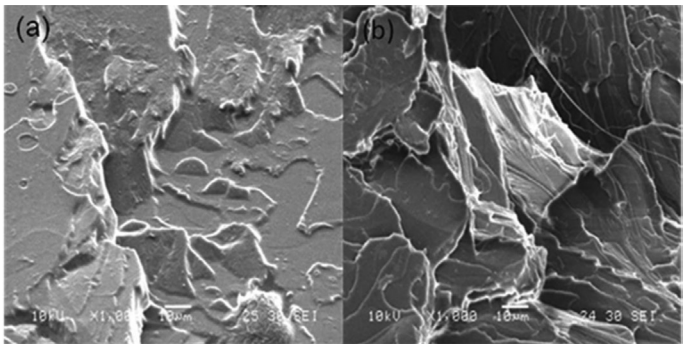

FIGURE 7. SEM micrographs of PLA-1DSNF biocomposite at 100× magnification

TABLE 5. Thermal analysis of PLA and PLA-1DSNF biocomposite

Sample	$T_{15\%}$ (°C)	T_f (°C)	Char residue (%) at 600°C
PLA	313	355	0.61
PLA-1DSNF	317	352	8.95

compound hydrogen and carbon atoms in the PLA-1DSNF chain as it decomposed completely at high temperature (Damadzadeh et al. 2010).

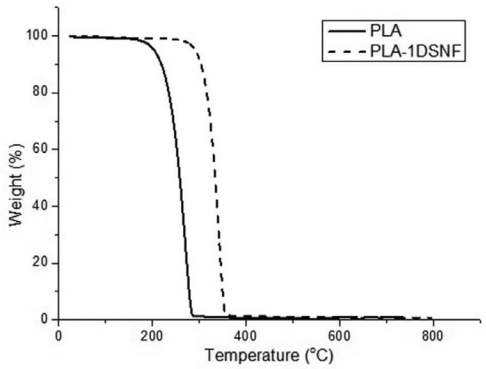

FIGURE 8. TG curves for PLA-1DSNF biocomposite

The thermal study was further analysed via DSC analysis of both composites (Table 6). Table 6 shows that the glass transition temperature (T_g), melting temperature (T_m) and cold crystallization temperature (T_{cc}) for biocomposite are slightly higher than in the PLA matrix. The effect of the filler content on the thermal properties of polylactide composites reported that the addition of filler increased the $T_{g.}$ (Ndiaye & Tidjani 2012). They relate the higher T_g caused by the restriction of the mobility of polymer chains to the presence of filler particles. It is noted in Table 6 that the addition of 1 wt. % DSNF significantly affects the crystallinity behaviour of PLA biocomposite. The higher crystallinity of the polymer composites indicates that the presence of a certain amount of filler tends to influence the interfacial bonding in the crystalline polymer and consequently the overall mechanical properties of the composite. This is in agreement with several studies on the DSC analysis of PLA and PLA composites, where the existence of cellulosic materials in the polymer matrix acts as a nucleating agent and promotes higher crystallinity (Shahzad, 2011; Siregar et al. 2012).

The DMA was performed on DSNF reinforced with PLA-1DSNF biocomposites sample. Figure 9(a)-9(b) illustrates the effect of DSNF on storage modulus and loss modulus of PLA/DSNF biocomposite in comparison with neat PLA sample. The crystallisation of PLA in the presence of different cellulose-based reinforcements has been studied progressively (Ho et al. 2012). They reported that the amorphous phase might restrict the chain mobility, which lead to the decrease of the stiffness of the composites. Based on Figure 9(a), PLA-1DSNF showed lower storage modulus (2.1 GPa) in comparison to neat PLA starting from the temperature around 50°C. This demonstrates the ease of deformation of the material by an applied load associated with the softening of PLA as the matrix as the temperature increased (Meng et al. 2011). The variation of loss modulus (Figure 9(b)) is used to measure glass transition temperature (T_g) for PLA and PLA-1DSNF biocomposites. From Figure 9(b), it can be observed that the peak of PLA-1DSNF biocomposite was slightly shifted down to lower temperature as compared to PLA at the transition region. This is dependent on the fibre length, fibre content and its interfacial adhesion that determines the maximum stress transfer between the fibre and the matrix. A broad transition (between 50 to 80°C)

TABLE 6. DSC analysis of PLA and PLA-1DSNF biocomposite

Sample	T_g (°C)	T_{cc} (°C)	T_m (°C)	ΔH_c (J/g)	ΔH_m (J/g)	Percentage of crystallinity (X%)
PLA	61.9	106.3	152.6	19.9	28.8	9.6
PLA-1DSNF	63.5	115.3	155.6	3.5	29.1	27.5

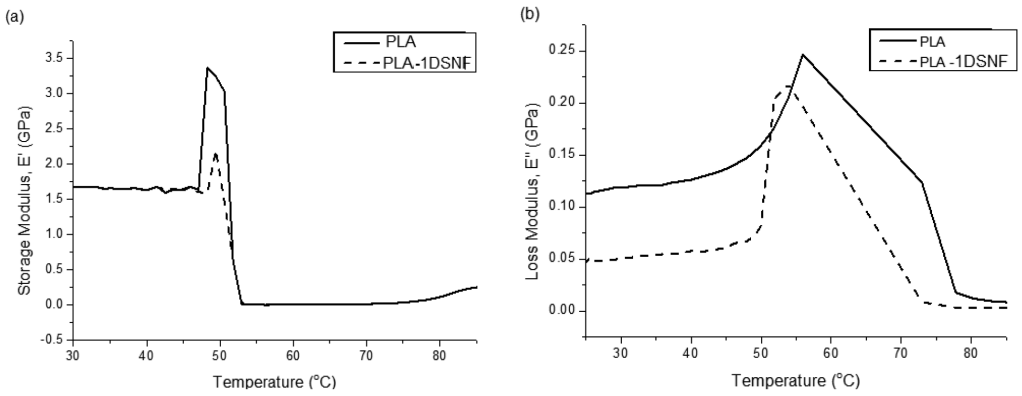

FIGURE 9. Variation of (a) storage modulus and (b) loss modulus as a function of temperature for PLA and PLA-1DSNF

for both samples was related to the cold crystallisation of PLA in this transition temperature region. From Figure 9(a)-9(b), the ratio of energy loss to energy retained in loading cycle was low due to the lower storage and loss modulus of PLA-1DSNF. The ratio of energy was low due to the presence of unevenly distributed DSNF along the matrix, which is also related to its uneven size.

CONCLUSION

Nanofibres with diameters in the range of 49 to 81 nm were biologically extracted from durian skin fibre. Only 1 wt. % of DSNF obtained significantly enhanced tensile properties and impact strength of PLA biocomposite. The higher $T_{15\%}$ of PLA-1DSNF biocomposite indicates that the thermal stability is improved with DSNF. The presence of DSNF also increased the T_g, T_{cc} and T_m of the PLA biocomposite. The presence of DSNF indicated lower storage modulus and loss modulus of PLA-1DSNF biocomposite. However, further improvements in nanofibre extraction and production can be made in order to broaden its utilization in the composite industry.

ACKNOWLEDGEMENTS

The authors wish to thank the Ministry of Education, Malaysia for its financial support through the Exploratory Research Grant Scheme (ERGS12-022-0022) and to the International Islamic University Malaysia and Universiti Putra Malaysia for the use of its facilities and equipment in making these studies a success.

REFERENCES

Albert, S., Padhiar, A. & Gandhi, D. 2011. Fiber properties of *Sorghum halepense* and its suitability for paper production. *J. Natural Fibers* 8: 263-271.

Atta, H.M. & Yassen, A.M. 2014. Phylogenetic characterization, fermentation and biological activities of an antibiotic producing *Streptomyces clavuligerus* isolated from KSA. *Int. J. Curr. Microbiol. App. Sci.* 3(12): 519-534.

Chen, W., Yu, H., Liu, Y., Hai, Y., Zhang, M. & Chen, P. 2011. Isolation and characterization of nanofibers from four plant cellulose fibers using chemical ultrasonic process. *Cellulose* 18: 433-442.

Damadzadeh, B., Jabari, H., Skrifvars, M., Airola, K., Moritz, N. & Vallitu, P.K. 2010. Effect of ceramic filler content on thermal and mechanical behaviour of poly-L-Lactic and poly-L-lactic-co-glycolic acid composites for medical applications. *Journal of Materials Science* 21: 2523-2531.

Dasong, D. & Mizi, F. 2010. Characteristics and performance of elementary hemp fiber. *Materials Sciences and Applications* 1: 336-345.

Eichhorn, S.J., Dufresne, A., Aranguren, M., Marcovich, N.E., Capadona, J.R. & Rowan, S.J. 2010. Review: Current international research into cellulose nanofibers and nanocomposites. *Mater. Science* 45: 1-33.

Ho, M., Wang, H., Lee, J.H., Ho, C.K., Lau, K., Leng, J. & Hui, D. 2012. Critical factors on manufacturing processes of natural fibre composites. *Composites Part B* 43: 3549-3562.

Ibrahim, M.M., Dufresne, A., El-Zawawya, W.K. & Aglebor, F.A. 2010. Banana fibers and microfibrils as lignocellulosic reinforcements in polymer composites. *Carbohydrate Polymers* 81: 811-819.

Isroi, Ria Millati, Siti Syamsiah, Claes Niklasson, Muhammad Nur Cahyanto, Knut Lundquist & Mohammad J. Taherzadeh. 2011. Biological pre-treatment of lignocelluloses with white rot fungi and its applications: A review. *Bioresources* 6(4): 5224-5259.

Janardhnan, S. & Sain, M. 2011. Targeted disruption of hydroxyl chemistry and crystallinity in natural fibers for isolation of cellulose nanofibers via enzymatic treatment. *Bioresources* 6: 1242-1250.

Jonoobi, M., Khazaeian, A., Tahir, P., Azry, S.S. & Oksman, K. 2011. Characteristics of cellulose nanofibers isolated from rubberwood and empty fruit bunches of oil palm using chemo-mechanical process. *Cellulose* 18: 1085-1095.

Kaiser, M.R., Anuar, H., Samat, A.N. & Abdul Razak, S. 2013. Effect of processing route on mechanical, thermal and morphological properties of PLA-based hybrid biocomposite. *Iranian Polymer Journal* 22(2): 123-131.

Kazimierczak, J., Bloda, A., Wietecha, J., Ciechanska, D. & Antczak, T. 2012. Research into isolation of cellulose micro and nanofibers from hemp straw using cellulolytic complex from *Aspergillus Niger*. *Fibres & Textiles in Eastern Europe* 6B(96): 40-43.

Kumar, P. & Awasthi, S. 2014. Mechanical and thermal modelling of ln-Cu composites for thermal interface materials applications. *Journal of Composite Materials* 48(11): 1391-1398.

Mamun, A.A. & Bledzki, A.K. 2013. Micro fibre reinforced PLA and PP composites: Enzyme modification, mechanical and thermal properties. *Composites Science and Technology* 78: 10-17.

Manshor, M.R., Anuar, H., Nur Aimi, M.N., Ahmad Fitrie, M.I., Wan Nazri, W.B., Sapuan, S.M., El-Shekeil, Y.A. & Wahit, M.U. 2014. Mechanical, thermal and morphological properties of durian skin fibre reinforced PLA biocomposites. *Materials and Design* 59: 279-286.

Meng, Q.K., Hetzer, M. & De Kee, D. 2011. PLA/clay/wood nanocomposites: Nanoclay effect on mechanical and thermal properties. *Journal of Composite Materials* 45(10): 1145-1158.

Mohammad, N.N.B. & Arsad, A. 2013. Mechanical, thermal and morphological study on kenaf fibre reinforced rpet/ABS composites. *Malaysian Polymer Journal* 8(1): 8-13.

Ndiaye, D. & Tidjani, A. 2012. Effects of coupling agents on thermal behaviour and mechanical properties of wood flour/polypropylene composites. *Journal of Composites Materials* 46(24): 3067-3075.

Nur Aimi, N., Anuar, H., Manshor, M.R., Wan Nazri, W.B. & Sapuan, S.M. 2014. Optimizing the parameters in durian skin fiber reinforced polypropylene composites by response surface methodology. *Industrial Crops and Products* 54: 291-295.

Nur Aimi, M.N., Mohd Adlan, M.K., Nurhafizah, S.M., Anuar, H., Mel, M. & Othman, R. 2011. Effect of *Rhizopus Oryzae* fermentation on kenaf based polylactic acid's monomer. *IIUM Engineering Journal (Special Issue on Biotechnology)* 12(4): 83-87.

Sahan, Y. 2011. Effect of *Prunus lauroceranus* L. (Chery Laurel), leaf extracts on bread spoilage fungi. *Bulgarian Journal of Agriculture Science* 17(1): 83-92.

Segal, L., Creely, J.J., Martin Jr., A.E. & Conrad, C.M. 1959. An empirical method for estimating the degree of crystallinity of native cellulose using the X-Ray diffractometer. *Textile Research Journal* 29: 786-794.

Shahzad, A. 2011. Hemp fibre and its composites - A review. *Journal of Composite Materials* 46(8): 973-986.

Siqueira, G., Bras, J. & Dufresne, A. 2010. Cellulosic bionanocomposites: A review of preparation, properties and applications. *Polymer* 2: 728-765.

Siregar, J.P., Sapuan, S.M., Rahman, M.Z.A. & Zaman, H.M.D.K. 2012. Effects of alkali treatments on the tensile properties of pineapple leaf fibre reinforced high impact polystyrene composites. *Pertanika Journal of Science and Technology* 20(2): 409-414.

Siyamak, S., Ibrahim, N.A., Abdolmohammadi, S., Wan Yunus, W.M.Z. & Rahman, A.B. 2012. Enhancement of mechanical and thermal properties of oil palm empty fruit bunch fibre poly(butylenesadipate-*co*-terephtalate) biocomposites by matrix esterification using succinic anhydride. *Molecules* 17(2): 1969-1991.

Tsukamoto, J., Duran, N. & Tasic, L. 2013. Nanocellulose and bioethanol production from orange waste using isolated microorganisms. *Journal of Brazilian Chemical Society* 24(9): 1537-1543.

M.N. Nur Aimi* & H. Anuar
Department of Manufacturing and Materials Engineering
Faculty of Engineering, International Islamic University Malaysia
P.O. Box 10, 50728 Kuala Lumpur, Wilayah Persekutuan
Malaysia

M. Maizirwan
Department of Biotechnology Engineering
Faculty of Engineering, International Islamic University Malaysia
P.O. Box 10, 50728 Kuala Lumpur, Wilayah Persekutuan
Malaysia

S.M. Sapuan
Department of Mechanical and Manufacturing Engineering
Universiti Putra Malaysia
43400 Serdang, Selangor Darul Ehsan
Malaysia

M.U. Wahit
Center for Composites
Universiti Teknologi Malaysia
81310 Skudai, Johor Darul Takzim
Malaysia

S. Zakaria
Materials Science Programme, School of Applied Physics
Faculty of Science and Technology
Universiti Kebangsaan Malaysia
43600 Bangi, Selangor Darul Ehsan
Malaysia

*Corresponding author; email: aimi_nasir@ymail.com

Received: 28 March 2015
Accepted: 22 June 2015